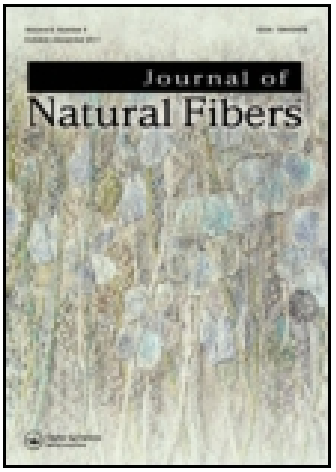

Journal of Natural Fibers
Publication details, including instructions for authors and subscription information:
http://www.tandfonline.com/loi/wjnf20

Composite Fiber Based on Sisal Fiber and Calcium Carbonate

Roberto C. Dante[a], F. M. Sánchez-Arévalo[b], L. Huerta[b], Pablo Martín-Ramos[a], Luis M. Navas-Gracia[a] & Jesús Martín-Gil[a]

[a] Laboratorio de Materiales y Tecnologías del Medio Ambiente, Departamento de Ingeniería Agrícola y Forestal, Universidad de Valladolid, Palencia, Spain

[b] Instituto de Investigaciones en Materiales, Universidad Nacional Autónoma de México, Cd. Universitaria, México, Mexico

Published online: 09 Apr 2014.

Journal of Natural Fibers, 11:121–135, 2014

ISSN: 1544-0478 print/1544-046X online
DOI: 10.1080/15440478.2013.849644

Taylor & Francis
Taylor & Francis Group

Composite Fiber Based on Sisal Fiber and Calcium Carbonate

ROBERTO C. DANTE,[1] F. M. SÁNCHEZ-ARÉVALO,[2] L. HUERTA,[2] PABLO MARTÍN-RAMOS,[1] LUIS M. NAVAS-GRACIA,[1] and JESÚS MARTÍN-GIL[1]

[1]*Laboratorio de Materiales y Tecnologías del Medio Ambiente, Departamento de Ingeniería Agrícola y Forestal, Universidad de Valladolid, Palencia, Spain*
[2]*Instituto de Investigaciones en Materiales, Universidad Nacional Autónoma de México, Cd. Universitaria, México, Mexico*

The impregnation of a raw sisal fiber in a saturated solution of calcium hydroxide generated a fiber coated by a remarkable quantity of calcium carbonate and calcium oxide. However, some detachments of the inorganic coating were observed at microscopic level, and interstices in the external walls, filled by the precipitated material, were less visible than in raw fiber. Additionally, some fiber components have been removed by the preliminary sodium silicate washing. The final composite exhibited more amorphous characteristics than the original raw fiber, as well as its mechanical behavior was very similar to an elastomeric material with more homogeneous mechanical properties than the original raw fiber.

KEYWORDS sisal, calcium silicate, composite fiber, natural fiber, calcium carbonate, hybrid fiber

浸渍在氢氧化钙的饱和溶液中的剑麻原麻纤维表面被大量的碳酸钙和氧化钙包覆。但是，在显微镜水平观察无机涂层，外墙的空隙，通过沉淀物的填充，跟原纤维比不那么明显。此外一些纤维成分已由初步硅酸钠洗涤除去。相比原来的粗纤维，最终的复合材料表现出更多的非晶特性，其机械性能类似，弹性材料的机械性能更均匀。

关键词：剑麻，硅酸钙，复合纤维，天然纤维，碳酸钙，复合纤维

Address correspondence to Roberto C. Dante, Laboratorio de Materiales y Tecnologías del Medio Ambiente, Departamento de Ingeniería Agrícola y Forestal, Universidad de Valladolid, Avenida de Madrid 44, 34004 Palencia, Spain. E-mail: rcdante@yahoo.com; lmnavas@iaf.uva.es

INTRODUCTION

Natural fibers such as sisal, is obtained from the leaves of agave sisaliana. This natural fibers have had a wide used in the past for ropes, bags, baskets, rugs, polishing cloths, and other textile manufactures, which required tough fibers (Li et al. 2000). The main disadvantages of synthetic fibers derived from petroleum, to substitute natural fibers are their performances and often are also their high prices. Synthetic inorganic fibers such as glass fiber, rock wool, and carbon fiber have found wide use in composite materials. However, natural fibers are being rediscovered for environmental reasons. They are renewable stuffs produced in areas of emerging economy. The advantage of industrial-scale production and mechanization process makes these fibers attractive again from a commercial standpoint (Technical paper n.14, 2000). New applications for the automotive industry, based in composite materials of either thermoplastic or thermosetting matrixes are being added to those traditional uses (Technical paper n.56, 2008).

Moreover, applications in the acoustic and thermal isolation fields are also being developed and the spin-off could have high impact in the building industry very soon. It is noteworthy to mention that natural fiber utilization is often due to the necessity to reduce the environmental impact of the products. To achieve this goal natural and renewable components have to be introduced in several industry branches. Indeed, natural fibers in automotive industry are relegated because are not able to resist high mechanical or thermal stresses. However, combining some of the properties of synthetic mineral fibers, which in spite of brittleness have a high thermal stability and low thermal conductivity (Korontahliova and Matiasovsky 2003), with those of natural fibers—such as deformability, flexibility, low thermal conductivity, and toughness—the latters can acquire an added value. This can allow to spread the use of natural fibers and the more expensive mineral fibers can be partially replaced (Santos Medeiros Neira and Santos Marinho 2009). That it is why research efforts were focused on the improvement and modification of the sisal fibers with different purposes (de Andrade Silva et al. 2010; Silva et al. 2010; Zhong et al. 2007). Zhong et al. applied alkali treatments as a reinforcing method, in order to obtain a composite fiber to be used in a urea formaldehyde resin matrix (Zhong et al. 2007); Silva et al. obtained a composite formed by the association of sisal fibers and a thermoset resin. They found that beneficial effects occur for composite fibers (Silva et al. 2010). Several efforts have been done too take advantage of composite sisal fibers and sisal fibers in composites. For example, thin cement-based laminates for semistructural and structural applications have been reinforced with Sisal fiber–cement composites with long unidirectional aligned fibers (de Andrade Silva et al. 2010).

Our work deals with the preparation of composite and hybrid natural fibers, starting from the aforementioned sisal fiber, through a simple method

of serial impregnations in inorganic salt solutions. The final product was a fiber, which kept the original morphology of the natural fiber, but with a coat of calcium carbonate (Sanders and Gallagher 2002). The product was characterized by several techniques, including infrared spectroscopy (IR), X-ray diffractometry (XRD), X-ray photoelectron spectroscopy (XPS), thermal gravimetric analysis (TGA), scanning electron microscopy (SEM), and tensile stress/strain analysis. The new product had chemical, mechanical, and thermal characteristics very different from the departure sisal fiber.

EXPERIMENTAL SECTION

Materials and Equipments

The composite fiber was obtained by impregnating 5 g of raw sisal short fibers (6–8 cm) supplied by Katani Ltd. (Tanzania), in a solution at 10% by weight of calcium silicate with molar ratio $SiO_2/NaO \sim 1$, supplied by Ingessil S.r.l. (Italy), for 24 h. Subsequently, the treated fiber was dried at 40°C for 24 h, and impregnated in a saturated solution of calcium hydroxide (lime) for other 24 h. The final drying was carried out in air at 40°C for 24 h. The obtained fiber had a yellowish color, in general, clearer than the departure fiber. A calcium carbonate sample was purchased from Sigma Aldrich with purity of 99.9% and used as reference in XPS analysis.

The specimens of both raw (*R*) and composite (*C*) fibers were analyzed by means of several techniques. Structure characteristics were obtained by means of XRD that was carried out by means of a Philips PW 1710 reflection diffractometer operating with Cu $K\alpha_1$ and $K\alpha_2$ radiations. Infrared (IR) spectra were obtained by means of Spectra Tech Nicolet 6700 in attenuated total reflectance (ATR) mode with diamond crystal, the chemical bond analysis was further studied through XPS. These measurements were carried out in an UHV system of VG Microtech ESCA2000 Multilab, with an Al $K\alpha$ X-ray source (1,486.60 eV), and a CLAM4 MCD analyzer. The surface of the samples was etched for 10 s with 3 $kVAr^+$ at 0.16 $\mu A/mm^2$. The XPS spectrum was obtained at 55° of the normal surface in the constant pass energy mode, $E_0 = 50$ eV and 200 eV for survey and high-resolution narrow scan, respectively. Peak positions were referenced to the background silver $3d_{5/2}$ photopeak at 368.20 eV, having a FWHM of 1.10 eV, Au $4f_{7/2}$ in 84.00 eV and C 1s hydrocarbon groups in 285.00 eV central peak position. XPS error was based on a detection limit estimated to be 0.1% and the uncertainty of deconvolution analysis was estimated to be 5%. The XPS spectra were fitted with the program SDP v 4.1 (SDP v4.1, 2004).

The morphology was investigated by means of an Amray 18301 Scanning Electron Microscope equipped with an energy-dispersive spectroscopy (EDS) probe. The thermal stability of the raw fiber was compared with that of the composite fiber by means of TGA, Mettler Toledo

TGA/SDTA851e/SF/1100, with differential thermal analysis DTA signal. Tensile mechanical experiments were carried out in custom-modified MTS load frame Minibionix 858 and its 407 MTS controller taking in to account the ASTM D3822-01 standard. The typical load cell used in this equipment (25 kN) was replaced by a 110 N interface load cell to get better measurements. The displacement signal was acquired from the LVDT sensor of the MTS machine. In order to register the force and displacement signals, a National Instruments PXI chassis and a NI-PXI 6285 board were used. The acquisition rate was 10,000 samples/s; so every small force variation was registered by a virtual instrument programmed in LabVIEW and a PC. The grips were specially designed and manufactured using stainless steel to hold the soft specimens firmly; additionally, special soft marks were machined between two plates of the grips to press the samples, thereby avoiding any sliding of the samples between plates. The tensile test parameters were: fiber length 25.4 mm, strain rate 25.4 mm/min at a 20°C. With the recorded displacement and force data, the macroscopic stress vs. strain ratio (λ-λ^{-2}) was obtained for each case. From these curves the shear modulus G was calculated in the linear region of the curves by linear square fitting. In order to calculate the Young Moduli of the sisal fibers, a conventional tensile test was used to obtain the stress as a function of strain. It is well known that the slope of this curve, in the elastic region, corresponds to the Young Modulus E. Nevertheless, when the materials exhibit an elastomeric behavior, the most appropriate way to determine the value of the Young modulus is through the stress as a function of strain ratio (λ-λ^{-2}) where $\lambda = \varepsilon + 1$, and ε is the engineering strain. Hence, the slope of the linear region where the fiber presents more resistance to tension is known as the shear modulus G. Considering this fact, we determined the Young modulus of sisal fibers assuming that $E = 3G$ for elastomeric materials (Jeon et al. 2007; Treloar 2005; Sánchez-Arévalo et al. 2010).

RESULTS AND DISCUSSION

Physical and Chemical Characterization

The IR spectra of samples R and C are shown in Figure 1. Sample R showed the typical bands of cellulose, such as the broad band due to the stretching of OH in interaction via hydrogen bond with a maximum at 3,325 cm^{-1}, These OHs belong to glucose rings, as well as to free water. Between 2,929 and 2,880 cm^{-1}, the asymmetric and symmetric stretching bands of the CH of glucose rings, as well as those of CH_2, bound to both the pyranose ring and OH, can be observed. It is also possible to observe the bending mode of absorbed water with peak at 1,604 cm^{-1}. The band around 1,400 cm^{-1} of sample R is due to modes of CH bending (Jia et al. 2011; Li et al. 2010), and at lower frequencies (wave numbers) there are other bands probably due

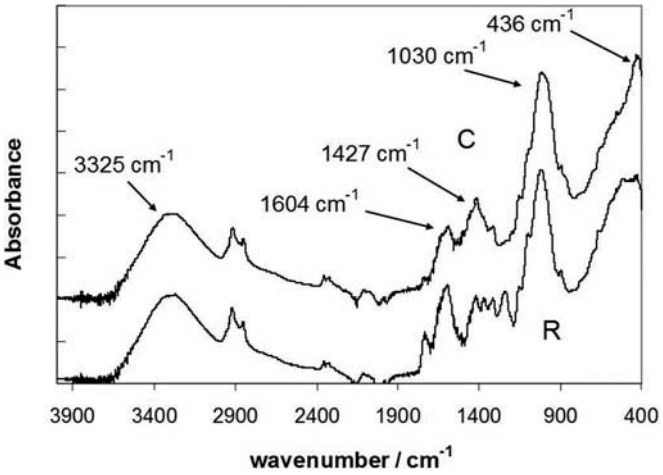

FIGURE 1 FT-IR spectra of *R* fiber and *C* fiber.

to modes of lignin. The characteristic stretching of carbonyl at 1,745 cm^{-1} can be due to esters, ketones, or aldehydes. The strong band at 1,030 cm^{-1}, present in both samples, is attributable to stretching CO of carbons bound to OH of the glucose units. The bands around 1,250 cm^{-1}, which can be due to CO stretching of lignin phenols, disappeared in sample *C*, indicating that the impregnations removed lignin.

In sample *C*, it is noteworthy to point out the presence of the band at 1,430 cm^{-1} which can be assigned to a stretching mode of calcium carbonate. The band at 436 cm^{-1} can be due to a bending mode of calcium carbonate too (http://webbook/nist/gov).

The TGAs of both samples (*R* and *C*) show the weight loss due to evaporation of absorbed water, which exhibits a well-shaped peak of DTA at 60°C (Figure 2), and that due to cellulose decomposition which starts from 250°C. The final residue at 900°C is 12.4 w% and 25.2 w% for samples *R* and *C*, respectively. Therefore, the amount of anhydrous and decomposed precipitated salts in sample C is 12.8 w%.

In order to understand the nature of chemical species and bonds, XPS analyses of the untreated *R* fiber and the treated *C* fiber were carried out. The core levels of C 1s, O 1s, and Ca 2p were considered. Figure 3 shows the survey spectra of *R* and *C* fibers, and it is possible to notice the presence of Si, and traces of N in addition to Ca, C and O.

Figure 4 shows high-resolution XPS spectra of C 1s of samples *C* and *R*, and that of $CaCO_3$ to be compared with the C 1s of the two fibers. The deconvolution of C 1s core peak shows three contributions in sample *R*, identified as: 1, 2, 3, which correspond to C–CH_2 of 285.00 eV, C–OH in 286.72 eV, and C–O–C in 288.31 eV, respectively. These three contributions correspond mainly to cellulose. It has been found also a very low content

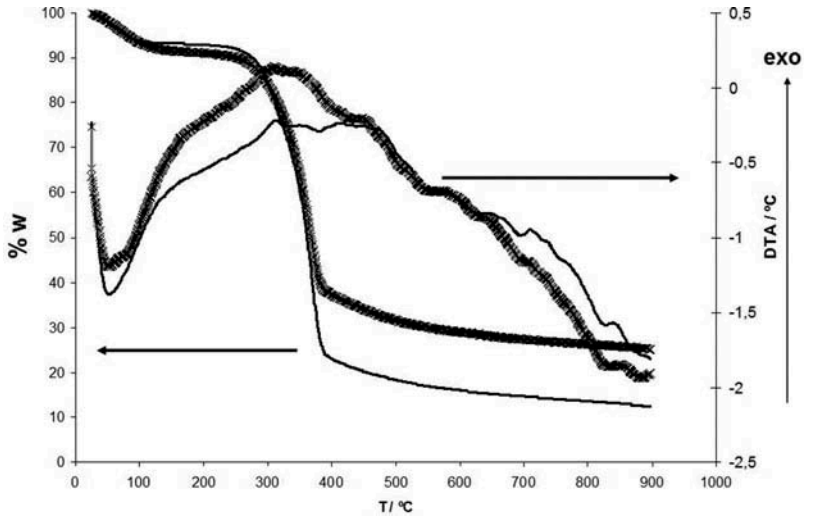

FIGURE 2 TGA and DTA signal of *R* fiber (thin line) and *C* fiber (thick line). The right arrow starts from the DTA curves and points toward the DTA ordinate axis, while the left arrow starts from the TGA curves and points towards the TGA axis.

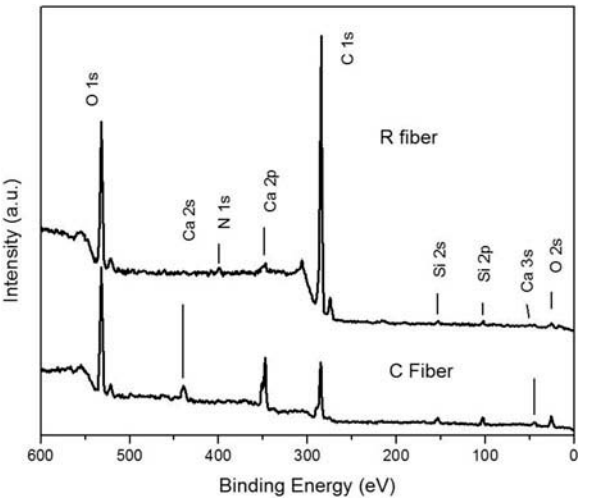

FIGURE 3 Survey XPS spectra of a raw *R* and composite *C* sisal fibers.

of C belonging to $CaCO_3$ at 289.91 eV (peak 4), the additional peak 5 at 285.00 eV may correspond to hydrocarbons: probably lignin, pectin, and fats (Beamson and Briggs 1992). It is noteworthy to point out that the spectrum of $CaCO_3$ exhibits a C 1s peak at 285.00 eV corresponding to pollutant hydrocarbons adsorbed by exposure to air. This fact is more evident because XPS is a technique of surface analysis. Sample *C* fiber was modified with a

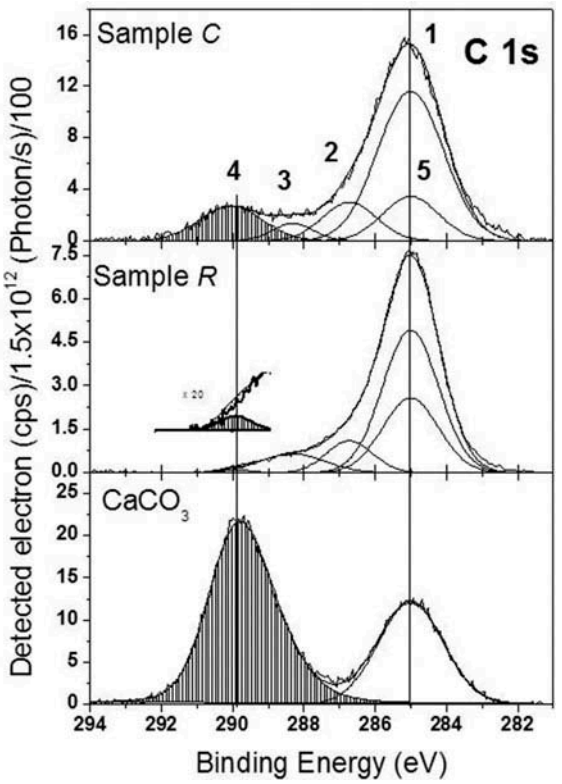

FIGURE 4 XPS spectra of C 1s core level: (a) Fiber *C*, (b) Fiber *R*, and (c) $CaCO_3$ powder. In the inset of fiber *R*, the peak of C1s belonging to $CaCO_3$ has been amplified by 20 times.

notable contribution of C belonging to $CaCO_3$. It can be seen that the amount of C belonging to $CaCO_3$ increased significantly from the percentage of 1% to 14% in substantial accordance with TGA measurements. Moreover, peak 5 attributed to lignin and cellulose decreased after washing with the sodium silicate solution in accordance with changes observed in IR spectra.

Figure 5 shows that in sample *R* the contributions of the O 1s core level to the fiber are four, two of which (peaks 1 and 2) concern the natural fiber as-is (sample *R*) and are identified as CH_2–OH at 533.14 eV and CH–O–CH at 532.24 eV, respectively; also there is the oxygen belonging to $CaCO_3$ at 531.36 eV (peak 3) (Christie et al. 1983), and the band at 531.29 eV (peak 4) may be attributed to O of CaO. Sample *C* contains the contributions of O 1s of both the natural fiber and $CaCO_3$ in the positions previously reported, and at 531.43 eV the contribution of O that may belong to CaO, stabilized by the cellulose matrix by specific interactions (Wagner et al. 1980). Actually, carbon carbonate is formed by reaction of CO_2 from air with the hydrated CaO forming a covering film.

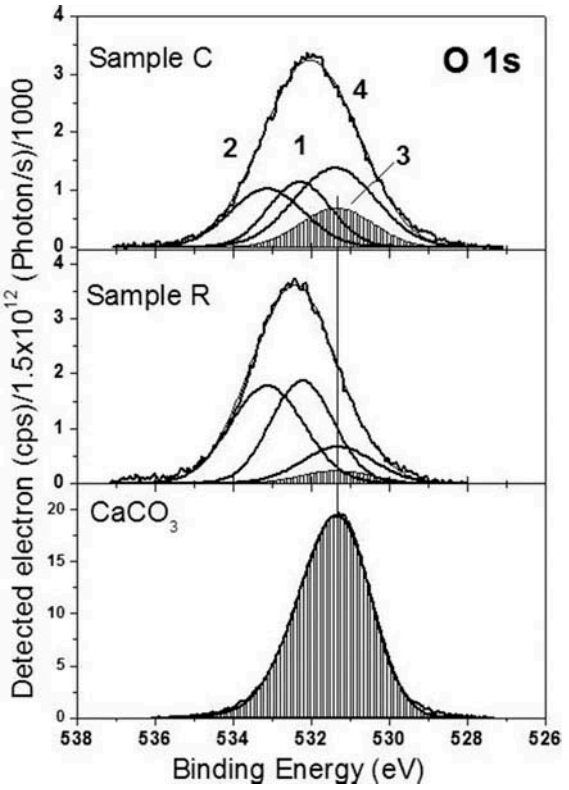

FIGURE 5 XPS spectra of O 1s core level: (a) Fiber *C*, (b) Fiber *R*, and (c) $CaCO_3$ powder.

Figure 6 shows the high-resolution XPS spectra of the core level of Ca 2p. Both samples *R* and *C* contain Ca of $CaCO_3$, as can been inferred by the presence of the deconvolution peaks of Ca $2p_{3/2}$ and Ca $2p_{1/2}$, at 347.04 eV and 350.53 eV, respectively (Jia et al. 2011). However, the calcium carbonate peaks are much more intense in fiber *C* than in fiber *R*. Moreover, fibers *R* and *C* have also a contribution of Ca $2p_{3/2}$ at 347.53 and 347.85 eV, respectively. In case of fiber *R*, this contribution may be due to Ca coming from the production process, and in case of fiber *C* may be due to the CaO not reacted with CO_2 (Demri and Muster 1995). All the assignments to the core level spectra of calcium carbonate, *R* and *C* samples are reported in Table 1.

The production process included washing fibers with a diluted lime solution and water after decortication, and a final drying by exposure of fibers to air and sun outdoor in country fields. During the washing phase, a certain contamination by calcium hydroxide, oxide and carbonate occurred. Calcium carbonate was presumably formed by reaction with CO_2 of air. It is noteworthy to point out that the amount of these compounds in fiber *R* is very low, and that XPS is substantially a surface analysis.

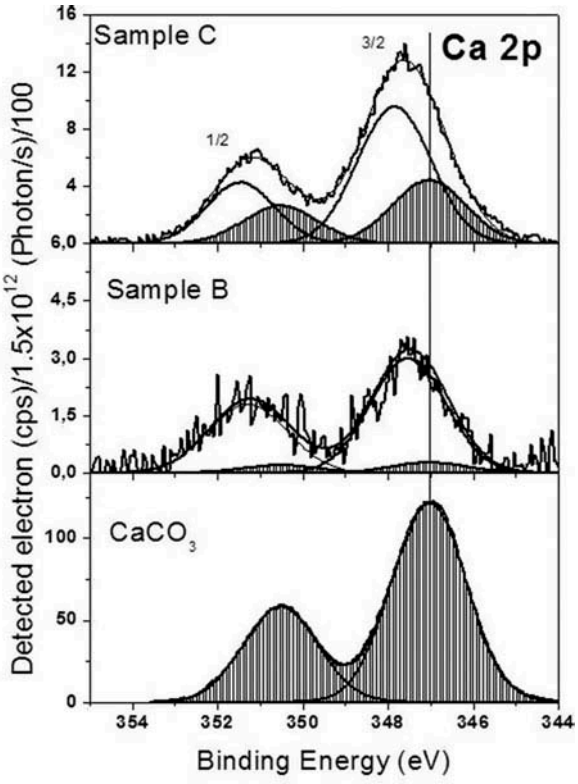

FIGURE 6 XPS spectra of Ca 2p 1s core level: (a) Fiber *C*, (b) Fiber *R*, and (c) $CaCO_3$ powder.

TABLE 1 Assignments to the core level (high resolution surface) XPS spectra of Fiber *R*, Fiber *C*, and $CaCO_3$ powder

	C 1s				O 1s				Ca $2p_{3/2}$	
Bond	$C–CH_2$	$CH_2–OH$	C–O–C	C of $CaCO_3$	$CH_2–OH$	C–O–C	O of $CaCO_3$	O of CaO	$CaCO_3$	CaO
Sample	Binding energy (eV)									
C	285.00	286.72	288.31	290.04	533.14	532.24	531.36	531.43	347.04	347.85
R	285.00	286.72	288.31	289.91	533.14	532.24	531.36	531.29	347.04	347.53
$CaCO_3$				287.34			531.36		347.04	

Structure and Morphology

X-ray diffraction patterns of *R* and *C* are shown in Figure 7. In the pattern of sample *R*, it is possible to distinguish the peaks of microcrystalline cellulose around 15.9° and 22°, in addition to other weak peaks around 35° and 46° (Jia et al. 2011). The diffraction pattern of *C* sample is less sharp than that of sample *R*. In addition, the peak, previously found at 22°, is shifted to 22.5°,

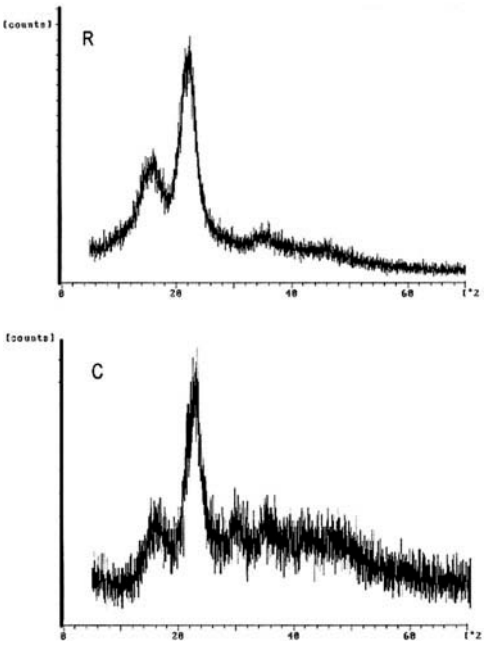

FIGURE 7 XRD patterns of *R* and *C* fibers XR.

and apart the same cellulose peaks, there are other weak and broad peaks at 29°, around 36°, 42°, and 46°. The precipitated salt in sample *C* generated a more amorphous material with less intense and broader peaks. The alteration of the characteristic peaks of cellulose indicates that the washing with the sodium silicate solution, as well as the precipitated inorganic salts further disordered the arrangement of cellulose chains. The broad peak at 29° may be correspond to microsrystalline calcium carbonate, in this case, this peak would correspond to the (104) reflection of calcite. (Ciobanu et al. 2010). Ciobanu et al. developed a composite of cellulose and calcium carbonate with a sharper peak at 29° typical of calcite. However, in their case the precipitate is crystalline (Ciobanu et al. 2010). In addition, this peak may also be due to microcrystalline calcium silicate formed for the washing with the sodium silicate solution or even to calcium hydroxide. A deep investigation is necessary to determine the presence of calcium carbonate with low crystallinity since it is well-known the high instability of amorphous calcium carbonate.

Figure 8 contains SEM images of samples *R* and of *C* at different magnifications, in which it is possible to observe the typical microstructure of sisal fibres. The external walls are smoother in the case of sample *R*. However, some particulates are observed, which may correspond to fragments of fiber or external inorganic particles, which came from the environment during the production process, as said previously.

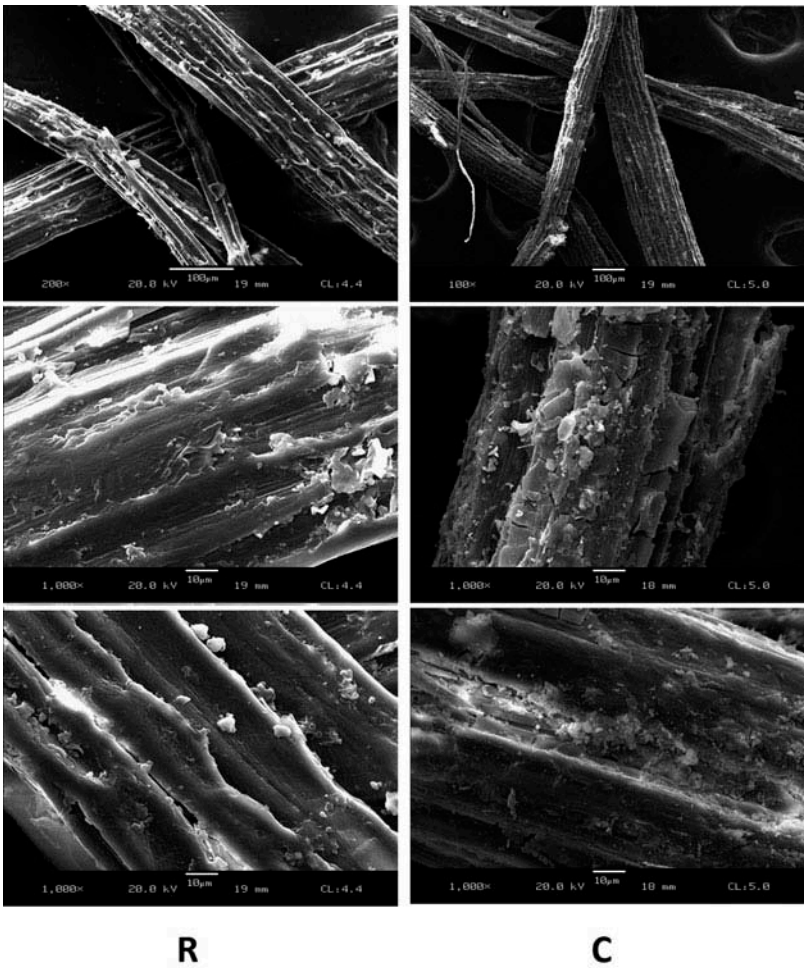

FIGURE 8 SEM images of *R* and *C* fibers.

The external walls of fibers *C* are wrinkled due to the many particles deposited and the irregularity of the coating material. Moreover, from the SEM images it can be inferred that the fiber diameter is around 100 μm. The composite fiber is covered by the mentioned inorganic coating which exhibits many cracks. In some cases, the detachment of the coating particles can be observed (see the image in the middle at right). Moreover, the scale structure of external walls is much less visible in fibers *C*, since the coating material occupied the interstices (see images at the bottom).

Mechanical Characterization

In Figure 9, the typical mechanical behavior of the natural *R* and treated *C* sisal fibers can be observed. This figure only contains the representative

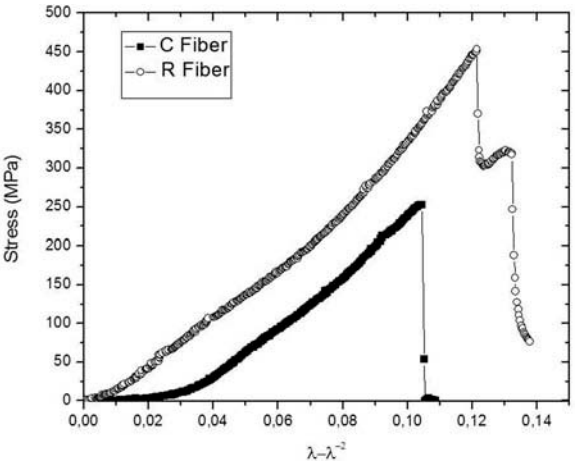

FIGURE 9 Typical Stress vs. λ-λ^{-2} curves for raw fiber *R* and coated sisal fiber *C*.

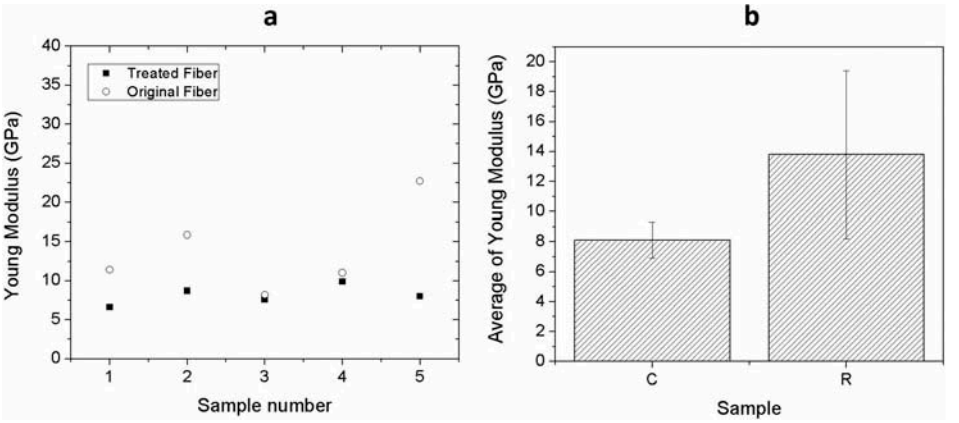

FIGURE 10 Young modulus of raw (original), *R*, and composite (treated), *C*, sisal fibers. (a) Young modulus of *R* and *C* samples, (b) Average of Young Modulus and their standard deviation for *R* and *C* samples.

behavior of both fibers. It has to be pointed out that five samples of each fiber were tested. As it can be realized the mechanical response of fiber *C* is especially very similar to the mechanical behavior of an elastomeric material with a flat initial region in the stress–strain curve. Furthermore, the slope of these curves, in the linear segment, corresponds to the shear module *G*. Hence, the Young modulus can be easily determined taking in to account the following expression $E = 3G$. It is noteworthy to point out that there are other methods to determine the shear modulus (Tsai and Daniel 1999).

Figures 10a and 10b show the Young modulus behavior of *R* and *C* fibers. The treated sisal *C* fibers presented an average Young module equal to 8.2 $\pm$ 1.2 GPa. While the raw natural fibers *R* showed the higher value

of 13.8 ± 5.6 GPa. Nevertheless, the dispersion in the second case was very high. The treatment applied to sisal fiber homogenized the mechanical behavior of this fiber notoriously but causing a decrement of the average Young modulus of *C* fibers.

CONCLUSIONS

The impregnation of a raw sisal fiber, previously washed with a solution of sodium silicate, in a saturated solution of calcium hydroxide generated a fiber coated by a remarkable quantity of calcium carbonate and calcium oxide, as shown by XPS and TGA analysis. The scale external walls of the fibers are much less visible in the composite fiber, since the coating materials occupied the interstices. However, the coating layer exhibited many cracks and some detachments of the inorganic coating were observed by SEM inspection. Some fiber components such as lignin were removed by the sodium silicate washing as evidenced by IR spectroscopy. Moreover, the final composite fiber exhibited a XRD pattern with more amorphous characteristics than the original raw fiber, and also there is a broad peak attributable either to microcrystalline calcite, either calcium hydroxide or calcium silicate. The mechanical behavior of the composite fiber was especially very similar to that of an elastomeric material with a marked initial flat region in the stress–strain curve, but with an average Young modulus lower than that of the raw fiber. This behavior can be explained by the mentioned removal of binding components such as lignin and the more amorphous state of the cellulose chains. Moreover, the mechanical properties seemed to be more homogeneous than those of the original raw fiber.

ACKNOWLEDGMENTS

We are very grateful to Dr. A. Tamashauski and all his group at Asbury Carbons (USA) for the SEM investigation.

REFERENCES

Beamson, G., and D. Briggs. 1992. *High resolution XPS of organic polymers*. New York: The Scienta ESCA300 Database, John Wiley and Sons.

Christie, A. B., J. LeeI, I. Sutherland, and J. M. Walls. 1983. An XPS study of ion-induced compositional changes with group II and group IV compounds. *Applied Surface Science* 15: 224–237.

Ciobanu, M., E. Bobu, and F. Ciolacu. 2010. In-situ cellulose fibres loading with calcium carbonate precipitated by different methods. *Cellulose Chemistry and Technology* 44: 379–387.

de Andrade Silva, F., R. Dias Toledo Filho, J. de almeida Melo Filho, and E. de Moraes REGO Fairbairn. 2010. Physical and mechanical properties of durable sisal fiber–cement composites. *Construction and Building Materials* 24: 777–785.

Demri, B., and D. Muster. 1995. XPS study of calcium compounds. *Journal of Materials Processing Technology* 55: 311–314. http://webbook.nist.gov/cgi/cbook.cgi?ID=C471341&Units=SI&Mask=80#Refs

Jeon, O., S. J. Song, K. Lee, M. H. Park, S. Lee, S. K. Hahn, S. Kim, and B. Kim. 2007. Mechanical properties and degradation behaviors of hyaluronic acid hydrogels cross-linked at various cross-linking densities. *Carbohydrate Polymers* 70: 251–257.

Jia, N., S. Li, M. Ma, and R. Sun. 2011. Microwave-assisted ionic liquid preparation and characterization of cellulose/calcium silicate nanocomposites in ethylene glycol. *Materials Letters* 65: 918–921.

Korontahliova, O., and P. Matiasovsky. 2003. Thermal conductivity of fiber reinforced calcium silicate hydrate-based materials. *Journal of Thermal Envelope and Building Science* 26: 71–89.

Li, S., N. Jia, J. Zhu, M. Ma, and R. Sun. 2010. Synthesis of cellulose–calcium silicate nanocomposites in ethanol/water mixed solvents and their characterization. *Carbohydrate Polymers* 80: 270–275.

Li, Y., Y. Mai, and L. Ye. 2000. Sisal fibre and its composites: A review of recent developments. *Composites Science and Technology* 60: 2037–2055.

Sánchez-Arévalo, F. M., M. Farfán, D. Covarrubias, R. Zenit, and G. Pulos. 2010. The micromechanical behavior of lyophilized glutaraldehyde-treated bovine pericardium under uniaxial tension. *Journal of the Mechanical Behavior of Biomedical Materials* 3: 640–646.

Sanders, J. P., and P. K. Gallagher. 2002. Kinetic analyses using simultaneous TG/DSC measurements Part I: Decomposition of calcium carbonate in Argon. *Thermochimica Acta* 388: 115–128.

Santos Medeiros Neira, D., and G. Santos Marinho. 2009. Non woven sisal fiber as thermal insulator material. *Journal of Natural Fibers* 6: 115–126.

SDP v4.1 (32 bit) Copyright© 2004, XPS International, LLC, Compiled in January 2004.

Silva, R. V., M. M. Ueki, D. Spinelli, W. W. Bose Filho, and J. R. Tarpani. 2010. Thermal Mechanical and hygroscopic behavior of sisal fiber/polyurethane resin-based composites. *Journal of Reinforced Plastics and Composites* 29: 1399–1417.

Technical paper n. 14, Common Fund for Commodities - Alternative Applications for Sisal and Henequen. *Proceedings of a Seminar held by the Food and Agriculture Organization of the UN (FAO) and the Common Fund for Commodities (CFC) Rome*, 13 Dec. 2000.

Technical paper n. 56, Discover Natural Fibre. *Proceedings of the Symposium on natural fibres*, Rome 20 Oct. 2008.

Treloar, L. R. G. 2005. *The physics of rubber elasticity*, Second Ed. New York: Oxford University Press.

Tsai, C. L., and I. M. Daniel. 1999. Determination of shear Modulus of single fibers. *Experimental Mechanics* 239: 284–286.

Wagner, C. D., D. A. Zatko, and R. H. Raymond. 1980. Use of the oxygen KLL Auger lines in identification of surface chemical states by electron spectroscopy for chemical analysis. *Analytical Chemistry* 52: 1445–1451.

Zhong, J. B., J. Lv, and C. Wei. 2007. Mechanical properties of sisal fibre reinforced urea- formaldehyde resin composites. *Express Polymer Letters* 1: 681–687.